

# Old & New in Strangeness Nuclear Physics

Avraham Gal

Racah Institute of Physics, The Hebrew University, 91904 Jerusalem, Israel  
avragal@savion.huji.ac.il

**Abstract.** Several persistent problems in strangeness nuclear physics are discussed in this opening talk at HYP2018, Norfolk VA, June 2018: (i) the  ${}^3_\Lambda\text{H}$ , and  ${}^3_\Lambda\text{n}$  if existing, lifetimes; (ii) charge symmetry breaking in  $\Lambda$  hypernuclei; (iii) the overbinding of  ${}^5_\Lambda\text{He}$  which might be related to the hyperon puzzle in neutron stars; and (iv) does  $\Lambda^*(1405)$  survive in strange hadronic matter?

## INTRODUCTION

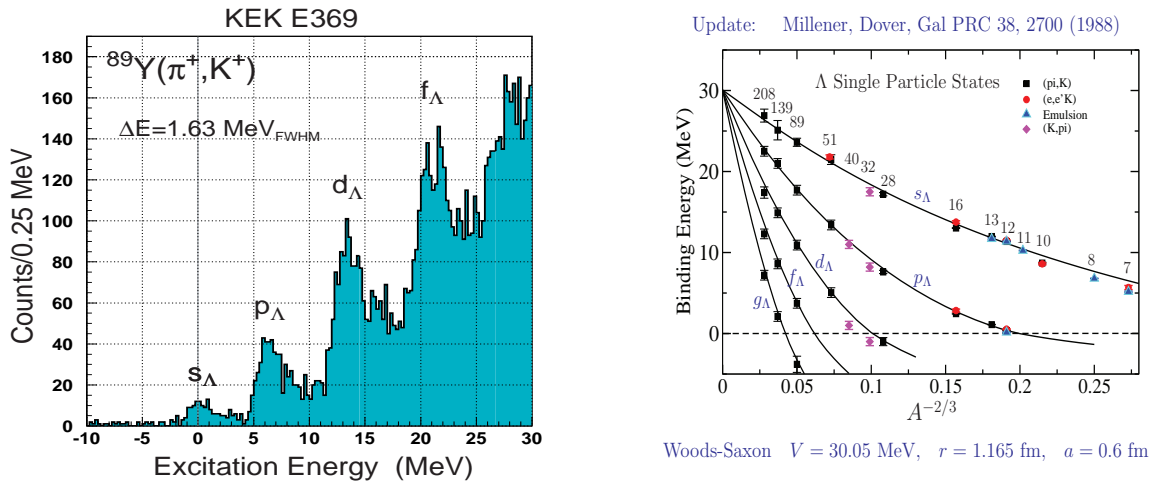


**FIGURE 1.** Left:  ${}^{89}\text{Y}(\pi^+, K^+)$  spectrum from KEK, exhibiting  $\Lambda$  single-particle orbits [2]. Right: compilation of  $\Lambda$  binding energies in  ${}^7_\Lambda\text{Li}$  to  ${}^{208}_\Lambda\text{Pb}$  from different reactions, and as calculated using a 3-parameter WS potential [3]. Figure adapted from Ref. [1].

Progress in Strangeness Nuclear Physics which 50 years ago consisted mostly of Hypernuclear Physics, with data collected exclusively in nuclear emulsions and bubble chambers, has been stepped up significantly with the advent of counter production experiments [1]. The left panel of Fig. 1 shows a  ${}^{89}\text{Y}(\pi^+, K^+)$  spectrum from KEK [2], exhibiting distinct  $\Lambda$  single-particle orbits in  ${}^{89}_\Lambda\text{Y}$  down to the ground-state (g.s.)  $s_\Lambda$  orbit, a feature unparalleled in ordinary nuclei and hence termed “a textbook example of a shell model at work” [3].

The right panel of Fig. 1 presents a compilation of most of the  $\Lambda$  hypernuclear binding energies ( $B_\Lambda$ ) measured across the periodic table as a function of  $A^{-2/3}$  and as fitted by a simple 3-parameter Woods-Saxon (WS) potential. The  $\Lambda$  nuclear potential well depth  $D_\Lambda$  in this simple-minded fit is 30 MeV, compared to  $27.8 \pm 0.3 \text{ MeV}$  from the 1988 first theoretical analysis [3] of the AGS  $(\pi^+, K^+)$  data [4]. Although the robustness of extrapolating to  $A \rightarrow \infty$  is primarily owing to the  $(\pi^+, K^+)$  production data in medium-weight and heavy nuclei, it is worth noting that  $D_\Lambda$  was derived more than 50 years ago, to less accuracy of course, from  $\pi^-$  decays of heavy spallation hypernuclei formed in silver and bromine emulsions [5, 6]:  $27 \pm 3 \text{ MeV}$  (1964) and  $27.2 \pm 1.3 \text{ MeV}$  (1965), respectively.

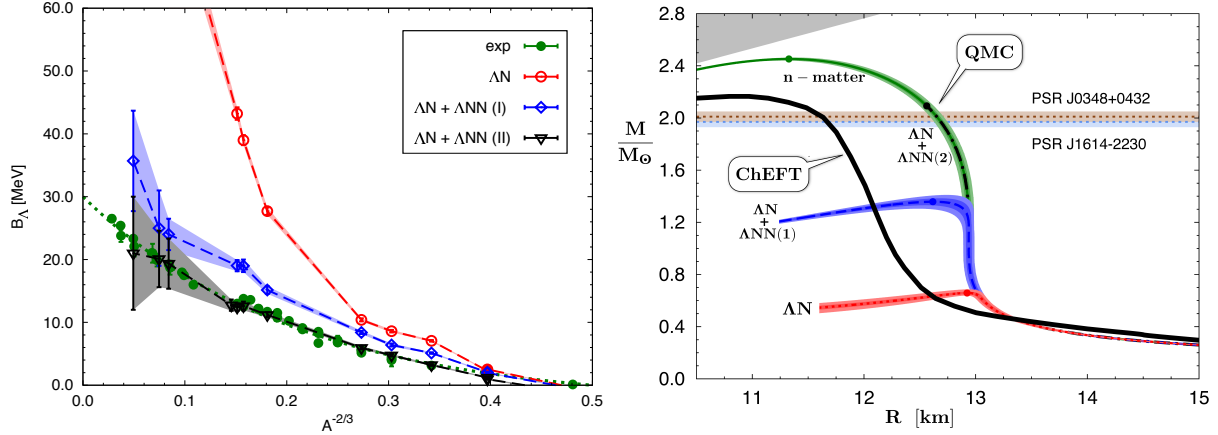


**FIGURE 2.** Left: QMC calculations of hypernuclear g.s.  $B_\Lambda$  values upon adding  $\Lambda NN$  interactions I and II [7]. Right: effect of adding  $\Lambda NN$  repulsive interactions I and II in neutron star calculations [8]. Figure adapted from Refs. [1, 9].

A well-depth value of  $D_\Lambda \sim 30$  MeV cannot be reproduced using two-body  $\Lambda N$  interactions exclusively. This was known already in 1988, with values about 50–60 MeV [3] derived using reasonable  $\Lambda N$  interactions, and is demonstrated perhaps in a somewhat exaggerated way in the left panel of Fig. 2 taken from recent quantum Monte Carlo (QMC) calculations by Lonardonì *et al.* [7]. These authors introduced phenomenological terms of repulsive  $\Lambda NN$  interactions motivated by coupling  $\Lambda N$  to  $\Sigma N$  channels and back to  $\Lambda N$  through one-pion exchange. The figure shows how by adding such terms and gradually strengthening their contribution (I to II), one is able to reproduce the empirical value of  $D_\Lambda \sim 30$  MeV. Implications of these results to neutron-star matter [8] are demonstrated in the right panel of Fig. 2, showing neutron-star mass-radius curves corresponding to the three  $B_\Lambda$  curves of the left panel. Adding  $\Lambda NN$  repulsion stiffens the equation of state of neutron-star matter such that, for the choice II,  $\Lambda$  hyperons are excluded and the experimentally deduced constraint  $M/M_\odot > 2$  is satisfied. Shown for comparison is a curve (ChEFT) involving nucleons and pions only [9]. This apparent solution of the so called ‘hyperon puzzle’ calls for more theoretically inclined work to confirm whether or not the puzzle has indeed been resolved.

The overbinding of  $\Lambda$  hypernuclei upon using exclusively two-body  $\Lambda N$  interactions was realized in the early 1970s, with Dalitz *et al.* [10] demonstrating unambiguously that such overbinding persists already in  $^5_\Lambda\text{He}$ , the lightest hypernucleus that is in fact a miniature of  $\Lambda$  in nuclear matter. This old problem motivated the new work on  $s$ -shell hypernuclei outlined in the next section and expanded in a contribution by Contessi *et al.* in this Volume.

Another topic discussed here, and separately by Andreas Nogga, is charge symmetry breaking (CSB) in  $\Lambda$  hypernuclei as demonstrated by the emulsion large value  $0.35 \pm 0.04$  MeV [11] of the binding energy difference  $B_\Lambda(^4_\Lambda\text{He}) - B_\Lambda(^4_\Lambda\text{H})$  which already in 1964 was realized to be as large,  $0.30 \pm 0.14$  MeV [12]. If a difference of two units in  $N - Z$  induces this large binding energy difference, what should one expect going to  $N - Z$  values as large as 44 in  $^{208}_\Lambda\text{Pb}$ ? The discussion of CSB in the  $p$  shell, updating my HYP2015 talk, partially answers this question.

A third topic, presented by Benjamin Dönigus at HYP2018 and discussed here, is the hypertriton lifetime puzzle: why is the lifetime of  $^3_\Lambda\text{H}$  so much shorter than the free  $\Lambda$  lifetime, as suggested in recent measurements using relativistic heavy ion collisions to produce light nuclei, anti-nuclei, and in particular loosely-bound and spatially-extended hyperfragments such as  $^3_\Lambda\text{H}$ ? Also discussed briefly is the lifetime expected for the questionable  $^3_\Lambda\text{n}$  hypernucleus.

Finally, we discuss here briefly the role of the dynamically generated  $\Lambda^*(1405)$ , a  $\bar{K}N$  quasibound state, in strange hadronic matter. For a more expanded discussion see the contribution by Hrtánková *et al.* in this Volume.

## OVERBINDING OF $^5_\Lambda\text{He}$

The overbinding of  $^5_\Lambda\text{He}$  upon using two-body  $\Lambda N$  interactions, and also upon adding  $\Lambda NN$  terms arising from the  $\Lambda N - \Sigma N$  coupling, was first recognized and stated clearly in a 1972 landmark paper by Dalitz *et al.* [10]. There, as well as in version I of the QMC calculations [7] (version II, instead, underbinds  $^3_\Lambda\text{H}$  and  $^4_\Lambda\text{H}$  [13]) and in recent leading-order (LO) chiral effective field theory ( $\chi\text{EFT}$ ) calculations [14], the  $\Lambda$  separation energy  $B_\Lambda(^5_\Lambda\text{He})$  comes out as large

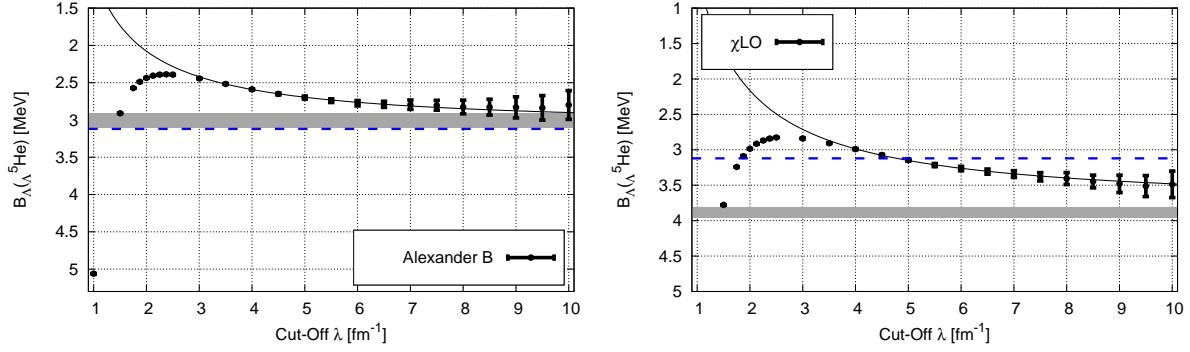


**FIGURE 3.**  $B_{\Lambda}({}^5_{\Lambda}\text{He})$  as a function of  $\lambda$  in  $\chi$ EFT calculations with  $\Lambda N$  input from  $\Lambda p$  scattering experiments [16] (left panel) and from a LO  $\chi$ EFT model [17] (right panel). Solid lines mark a fit  $a + b/\lambda$  for  $\lambda \geq 4 \text{ fm}^{-1}$ . Horizontal bands mark  $\lambda \rightarrow \infty$  extrapolation uncertainties. Dashed horizontal lines mark the value  $B_{\Lambda}^{\text{exp}}({}^5_{\Lambda}\text{He}) = 3.12 \pm 0.02 \text{ MeV}$ . Figure adapted from Ref. [15].

as 6 MeV, well above the measured value  $B_{\Lambda}^{\text{exp}}({}^5_{\Lambda}\text{He}) = 3.12 \pm 0.02 \text{ MeV}$ .

Contessi *et al.* [15] revisited recently the overbinding problem by doing stochastic variational method (SVM) precise calculations of  $s$ -shell hypernuclei, using Lagrangians constructed at LO in a pionless effective field theory ( $\chi$ EFT) approach limited to nucleons and  $\Lambda$ -hyperon degrees of freedom:

$$\mathcal{L} = N^\dagger (i\partial_0 + \frac{\nabla^2}{2M_N}) N + \Lambda^\dagger (i\partial_0 + \frac{\nabla^2}{2M_\Lambda}) \Lambda + \mathcal{L}_{2B} + \mathcal{L}_{3B} + \dots, \quad (1)$$

where  $\mathcal{L}_{2B}, \mathcal{L}_{3B}, \dots$  are two-body, three-body, etc., interaction terms composed of nucleon and  $\Lambda$  fields and their derivatives subject to symmetry constraints that  $\mathcal{L}$  is scalar and isoscalar and to a power counting which at LO limits these interaction terms to contact two-body and three-body  $s$ -wave interaction terms. These contact terms are regularized then by introducing a local Gaussian regulator with momentum cutoff  $\lambda$ . Apart from the two-body contact terms that are specified by  $NN$  and  $\Lambda N$  spin-singlet and triplet scattering lengths, amounting to four low-energy constants (LECs), the theory uses additionally four three-body LECs: a pure  $NNN$  LEC fitted to  $B({}^3\text{H})$  and three  $\Lambda NN$  LECs associated with the three possible  $s$ -wave  $\Lambda NN$  systems, of which only  ${}^3_{\Lambda}\text{H}(I=0, J^P=\frac{1}{2}^+)$  is bound. Therefore, on top of fitting its binding energy, the binding energies of  ${}^4_{\Lambda}\text{H}_{\text{g.s.}}(I=\frac{1}{2}, J^P=0^+)$  and of  ${}^4_{\Lambda}\text{H}_{\text{exc}}(I=\frac{1}{2}, J^P=1^+)$  are also fitted. The fitted LECs are used then, for a sequence of  $\lambda$  cutoff values, to evaluate the binding energies of  ${}^4\text{He}$  and  ${}^5_{\Lambda}\text{He}$ .

This  $\chi$ EFT approach was applied in SVM few-body calculations to the  $s$ -shell nuclei and in several models of the  $\Lambda N$  scattering lengths also to the  $s$ -shell hypernuclei. The resulting  $\Lambda$  separation energy values  $B_{\Lambda}({}^5_{\Lambda}\text{He})$  are shown in Fig. 3 for two such models as a function of the cutoff  $\lambda$ . Common to all  $\Lambda N$  models, the calculated  $B_{\Lambda}({}^5_{\Lambda}\text{He})$  values switch from about 2–3 MeV overbinding at  $\lambda=1 \text{ fm}^{-1}$  to less than 1 MeV underbinding between  $\lambda=2$  and  $3 \text{ fm}^{-1}$ , and smoothly varying beyond, approaching a finite (renormalization scale invariance) limit at  $\lambda \rightarrow \infty$ . A reasonable choice of *finite* cutoff values in the present case is between  $\lambda \approx 1.5 \text{ fm}^{-1}$ , which marks the  $\chi$ EFT breakup scale of  $2m_\pi$ , and  $4 \text{ fm}^{-1}$ , beginning at which the detailed dynamics of vector-meson exchanges may require attention.

The sign and size of the three-body contributions play a crucial role in understanding the cutoff  $\lambda$  dependence of the calculated  $B_{\Lambda}({}^5_{\Lambda}\text{He})$ . The nuclear  $NNN$  term first changes from weak attraction at  $\lambda=1 \text{ fm}^{-1}$  in  ${}^3\text{H}$  and  ${}^4\text{He}$ , similar to that required in phenomenological models [18], to strong repulsion at  $\lambda=2 \text{ fm}^{-1}$ , which reaches maximal values around  $\lambda=4 \text{ fm}^{-1}$ . However, for larger values of  $\lambda$  it decreases slowly. The  $\Lambda NN$  contribution follows a similar trend, but it is weaker than the  $NNN$  contribution by a factor of roughly 3 when repulsive. The transition of the three-body contributions from long-range weak attraction to relatively strong repulsion for short-range interactions is correlated with the transition seen in Fig. 3 from strongly overbinding  ${}^5_{\Lambda}\text{He}$  to weakly underbinding it. We note that for  $\lambda \gtrsim 1.5 \text{ fm}^{-1}$  all of the three  $\Lambda NN$  components are repulsive, as required to avoid Thomas collapse, imposing thereby some constraints on the  $\Lambda NN$  LECs.

Momentum-dependent interaction terms, such as tensor and spin-orbit, which appear at subleading order in  $\chi$ EFT power counting, will have to be introduced in future applications to  $p$ -shell hypernuclei. The long-range  $\Lambda N$  tensor force induced by a  $\Lambda N \rightarrow \Sigma N$  one-pion exchange (OPE) transition followed by a  $\Sigma N \rightarrow \Lambda N$  OPE transition is

expected to be weak because this two-pion exchange mechanism is dominated by its central  $S \rightarrow D \rightarrow S$  component, which is partially absorbed in the  $\Lambda N$  and  $\Lambda NN$  LO contact LECs. Short-range  $K$  and  $K^*$  meson exchanges induce a mild  $\Lambda N$  tensor force [19, 20], the weakness of which is confirmed in shell-model studies of observed  $p$ -shell  $\Lambda$  hypernuclear spectra [21]. Recent LO  $\chi$ EFT calculations [22] using induced  $YNN$  repulsive contributions suggest that the  $s$ -shell overbinding problem extends to the  $p$  shell. In contrast, shell-model studies [21] reproduce satisfactorily  $p$ -shell ground-state  $B_\Lambda$  values, essentially by using  $B_\Lambda^{\text{exp}}(^9\Lambda\text{He})$  for input, except for the relatively large difference of about 1.8 MeV between  $B_\Lambda(^9\Lambda\text{Li})$  and  $B_\Lambda(^9\Lambda\text{Be})$ . In fact, it was noted long ago that strongly repulsive  $\Lambda NN$  terms could settle it [23]. It would be interesting to apply our derived  $\Lambda NN$  interaction terms in future shell-model calculations.

Finally, the  $\chi$ EFT Lagrangian used here includes already at LO repulsive  $\Lambda NN$  terms which are qualitatively as strong as those used by Lonardoni, Pederiva and Gandolfi [7] to resolve the hyperon puzzle [8]. It would be interesting then to apply our  $\Lambda N + \Lambda NN$  interaction terms in state-of-the-art neutron-star matter calculations to see whether or not their suggested resolution of the hyperon puzzle is sufficiently robust.

## CHARGE SYMMETRY BREAKING

Charge symmetry breaking (CSB) is particularly strong in the  $A = 4$  mirror hypernuclei  $^4_\Lambda\text{H} - ^4_\Lambda\text{He}$ , as shown in Fig. 4. Although OPE does not contribute directly to the  $\Lambda N$  strong interaction owing to isospin invariance, it does contribute as pointed out by Dalitz and Von Hippel (DvH) through a CSB potential  $V_{\text{CSB}}^{\text{OPE}}$  generated by admixing the SU(3) octet  $\Lambda_{I=0}$  and  $\Sigma_{I=1}^0$  hyperons in the physical  $\Lambda$  hyperon [28]. For the mirror  $^4_\Lambda\text{H} - ^4_\Lambda\text{He}$  ground-state (g.s.) levels built on the  $^3\text{H} - ^3\text{He}$  cores, and using the DvH purely central wavefunction, the OPE CSB contribution amounts to  $\Delta B_\Lambda^{J=0} \approx 95$  keV where  $\Delta B_\Lambda^J \equiv B_\Lambda^J(^4\Lambda\text{He}) - B_\Lambda^J(^4\Lambda\text{H})$ . This was confirmed recently by Gazda and Gal using  $A=4$  wavefunctions generated within a LO  $\chi$ EFT no-core shell-model (NCSM) calculation [29] in which the OPE tensor interaction adds  $\approx 100$  keV [30]. Remarkably, the OPE overall contribution of  $\approx 200$  keV to the CSB splitting of the  $^4_\Lambda\text{H} - ^4_\Lambda\text{He}$  mirror g.s. levels roughly agrees with the large observed g.s. CSB splitting  $\Delta B_\Lambda^{J=0} = 233 \pm 92$  keV shown in Fig. 4 which is considerably larger than the approximately 70 keV CSB part of the 764 keV Coulomb-dominated binding-energy difference of the  $^3\text{H} - ^3\text{He}$  core mirror nuclei, driven apparently via short-range  $\rho - \omega$  mixing.

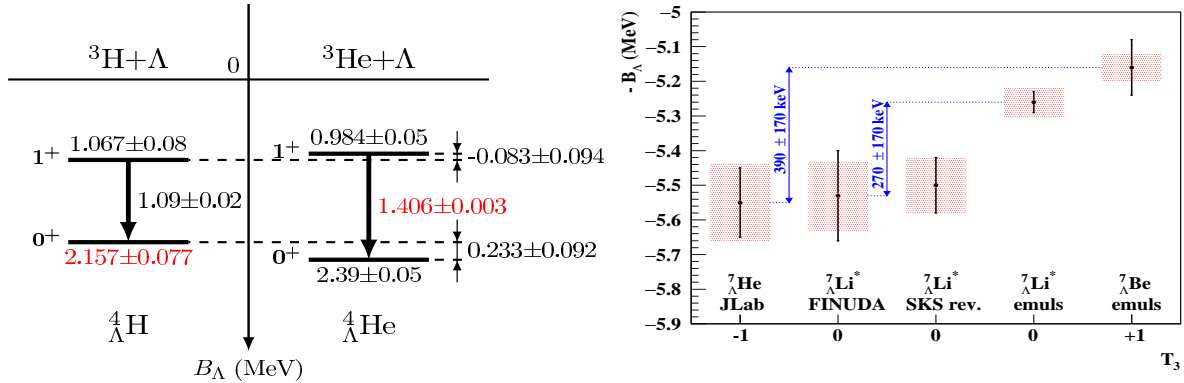


**FIGURE 4.** Left:  $A = 4$  hypernuclear level diagram. Recent determinations of the  $^4_\Lambda\text{He}$  excitation energy  $E_\gamma(1^+_{\text{exc}} \rightarrow 0^+_{\text{g.s.}})$  from J-PARC [24] and of the  $^4_\Lambda\text{H}$   $0^+_{\text{g.s.}}$  binding energy from MAMI [25, 26] are marked in red. CSB splittings are shown to the right of the  $^4_\Lambda\text{He}$  levels; figure adapted from Ref. [26]. Right:  $A = 7$  hypernuclear  $J^\pi = \frac{1}{2}^+$   $I = 1$  level diagram adapted from Ref. [27]. CSB splittings are relatively small if derived from *either* counter experiments *or* emulsion exposures.

In addition to OPE,  $\Lambda - \Sigma^0$  mixing affects also short-range meson exchanges (e.g., vector mesons) that in  $\chi$ EFT are replaced by contact terms. Quite generally, in baryon-baryon models that include *explicitly* a charge-symmetric (CS)  $\Lambda N \leftrightarrow \Sigma N$  ( $\Lambda\Sigma$ ) coupling, the direct  $\Lambda N$  matrix element of  $V_{\text{CSB}}$  is obtained from a strong-interaction CS  $\Lambda\Sigma$  coupling matrix element  $\langle N\Sigma | V_{\text{CS}} | N\Lambda \rangle$  by

$$\langle N\Lambda | V_{\text{CSB}} | N\Lambda \rangle = -0.0297 \tau_{Nz} \frac{1}{\sqrt{3}} \langle N\Sigma | V_{\text{CS}} | N\Lambda \rangle, \quad (2)$$

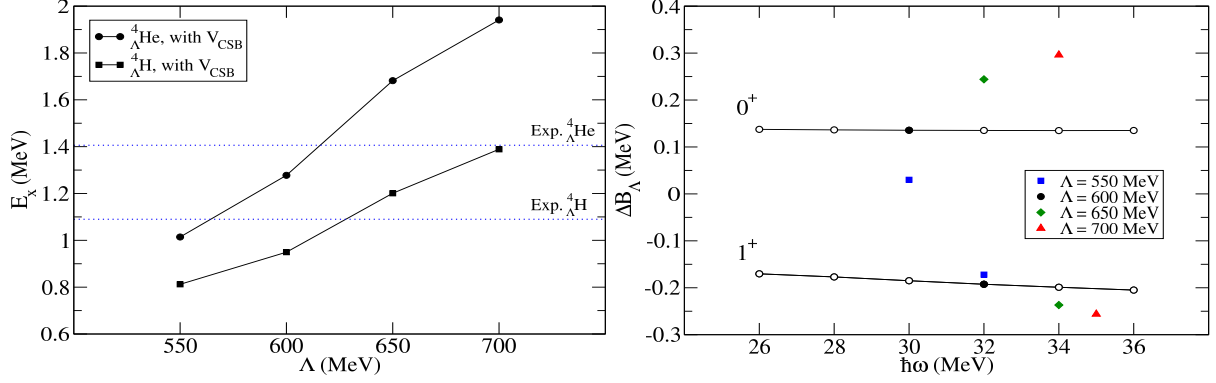


**FIGURE 5.** NCSM calculations of  ${}^4_\Lambda\text{H}$  and  ${}^4_\Lambda\text{He}$ , using CS LO  $\chi\text{EFT}$   $YN$  interactions [17] and  $V_{\text{CSB}}$ , Eq. (2), derived from these CS interactions. Left: momentum cutoff dependence of excitation energies  $E_x(0_{\text{g.s.}}^+ \rightarrow 1_{\text{exc}}^+)$ . The  $\gamma$ -ray measured values of  $E_x$  from Fig. 4 are marked by dotted horizontal lines. Right: HO  $\hbar\omega$  dependence, for  $\Lambda=600$  MeV, of the separation-energy differences  $\Delta B_\Lambda^J$  for  $0_{\text{g.s.}}^+$  (upper curve) and for  $1_{\text{exc}}^+$  (lower curve). Results for other values of  $\Lambda$  are shown at the respective absolute variational energy minima. Figure adapted from Ref. [30].

where the  $z$  component of the nucleon isospin Pauli matrix  $\vec{\tau}_N$  assumes the values  $\tau_{Nz} = \pm 1$  for protons and neutrons, respectively, the isospin Clebsch-Gordan coefficient  $1/\sqrt{3}$  accounts for the  $N\Sigma^0$  amplitude in the  $I_{NY} = 1/2$   $N\Sigma$  state, and the space-spin structure of this  $N\Sigma$  state is taken identical to that of the  $N\Lambda$  state sandwiching  $V_{\text{CSB}}$ . The 3% CSB scale factor  $-0.0297$  in Eq. (2) follows by evaluating the  $\Lambda - \Sigma^0$  mass mixing matrix element  $\langle \Sigma^0 | \delta M | \Lambda \rangle$  from SU(3) mass formulae [28, 31].

Since the CSB  $\Lambda N$  matrix element in Eq. (2) is given in terms of strong-interaction CS  $\Lambda\Sigma$  coupling, it is interesting to see how strong the latter is in realistic microscopic  $YN$  interaction models. Recent four-body calculations of  ${}^4_\Lambda\text{He}$  levels [32], using the Bonn-Jülich LO  $\chi\text{EFT}$  SU(3)-based  $YN$  CS potential model [17], show that almost 40% of the  $0_{\text{g.s.}}^+ \rightarrow 1_{\text{exc}}^+$  excitation energy  $E_x$  arises from  $\Lambda\Sigma$  coupling. This also occurs in the NSC97 models [33] as demonstrated by Akaishi *et al.* [34]. With  $\Lambda\Sigma$  matrix elements of order 10 MeV, the 3% CSB scale factor in Eq. (2) suggests a CSB splitting  $\Delta E_x \equiv E_x({}^4_\Lambda\text{He}) - E_x({}^4_\Lambda\text{H}) \sim 300$  keV, in good agreement with the splitting  $\Delta E_x^{\text{exp}} = 320 \pm 20$  keV [24] deduced from the r.h.s. of Fig. 4.

Results of the Gazda-Gal four-body NCSM calculations of the  $A=4$  hypernuclei [29, 30], using the Bonn-Jülich model [17] with momentum cutoff in the range  $\Lambda=550$ –700 MeV, are shown in Fig. 5. Plotted on the l.h.s. are the calculated  $0_{\text{g.s.}}^+ \rightarrow 1_{\text{exc}}^+$  excitation energies in  ${}^4_\Lambda\text{H}$  and in  ${}^4_\Lambda\text{He}$ , both of which are found to increase with  $\Lambda$  such that somewhere between  $\Lambda=600$  and 650 MeV the  $\gamma$ -ray measured values of  $E_x$  are reproduced. The  $\Lambda - \Sigma^0$  mixing CSB splitting  $\Delta E_x$  obtained by using Eq. (2) also increases with  $\Lambda$  such that for  $\Lambda=600$  MeV the calculated value  $\Delta(\Delta B_\Lambda) \equiv \Delta B_\Lambda^{\text{calc}}(0_{\text{g.s.}}^+) - \Delta B_\Lambda^{\text{calc}}(1_{\text{exc}}^+) = 330 \pm 40$  keV derived from the r.h.s. of the figure agrees with  $\Delta E_x^{\text{exp}}$ .

Plotted on the r.h.s. of Fig. 5 is the  $\hbar\omega$  dependence of  $\Delta B_\Lambda^J$ , including  $V_{\text{CSB}}$  from Eq. (2) and using  $N_{\text{max}} \rightarrow \infty$  extrapolated values for each of the four possible  $B_\Lambda^J$  values calculated at cutoff  $\Lambda=600$  MeV. Extrapolation uncertainties for  $\Delta B_\Lambda^J$  are 10 to 20 keV.  $\Delta B_\Lambda^{J=0}$  varies over the spanned  $\hbar\omega$  range by a few keV, whereas  $\Delta B_\Lambda^{J=1}$  varies by up to  $\sim 30$  keV. Figure 5 demonstrates a strong (moderate) cutoff dependence of  $\Delta B_\Lambda^{J=0}$  ( $\Delta B_\Lambda^{J=1}$ ):

$$\Delta B_\Lambda^{J=0} = 177_{-147}^{+119} \text{ keV}, \quad \Delta B_\Lambda^{J=1} = -215_{-41}^{+43} \text{ keV}. \quad (3)$$

The opposite signs and roughly equal sizes of these  $\Delta B_\Lambda^J$  values follow from the dominance of the  ${}^1S_0$  contact term (CT) in the  $\Lambda\Sigma$  coupling potential of the LO  $\chi\text{EFT}$   $YN$  Bonn-Jülich model [17], whereas the PS SU(3)-flavor octet ( $8_f$ ) meson-exchange contributions are relatively small and of opposite sign to that of the  ${}^1S_0$  CT contribution. This paradox is resolved by noting that regularized pieces of Dirac  $\delta(\mathbf{r})$  potentials that are discarded in the classical DvH treatment survive in the LO  $\chi\text{EFT}$  PS meson-exchange potentials. Suppressing such a zero-range regulated piece of CSB OPE within the full LO  $\chi\text{EFT}$   $A=4$  hypernuclear wavefunctions gives [30]

$$\text{OPE(DvH)} : \quad \Delta B_\Lambda^{J=0} \approx 175 \pm 40 \text{ keV}, \quad \Delta B_\Lambda^{J=1} \approx -50 \pm 10 \text{ keV}, \quad (4)$$

with smaller momentum cutoff dependence uncertainties than in Eq. (3). Both Eqs. (3) and (4) agree within uncertainties with the CSB splittings  $\Delta B_\Lambda^J$  marked in Fig. 4.

To apply the CSB procedure defined by Eq. (2) to  $p$ -shell hypernuclei, one introduces effective CS  $\Lambda\Sigma$  central interactions with  $p$ -shell  $0p_N 0s_Y$  matrix elements  $\bar{V}_{\Lambda\Sigma}^{0p}$  and  $\Delta_{\Lambda\Sigma}^{0p}$  listed in the caption to Table 1. These matrix elements follow from the shell-model reproduction of hypernuclear  $\gamma$ -ray transition energies by Millener [21] and are smaller by a factor roughly two than the corresponding  $s$ -shell  $0s_N 0s_Y$  matrix elements, thereby resulting in smaller  $\Sigma$  hypernuclear admixtures and implying that CSB contributions in the  $p$  shell are weaker with respect to those in the  $A = 4$  hypernuclei also by a factor of two, as demonstrated in Fig. 4. To evaluate  $p$ -shell CSB contributions, the single-nucleon expression (2) is extended by summing over  $p$ -shell nucleons [31]:

$$V_{\text{CSB}} = -0.0297 \frac{1}{\sqrt{3}} \sum_j (\bar{V}_{\Lambda\Sigma}^{0p} + \Delta_{\Lambda\Sigma}^{0p} \vec{s}_j \cdot \vec{s}_Y) \tau_{jz}. \quad (5)$$

Results of applying this effective  $\Lambda\Sigma$  coupling model to several pairs of g.s. levels in  $p$ -shell hypernuclear isomultiplets are given in Table 1, adapted from Ref. [35]. All pairs except for  $A = 7$  are g.s. mirror hypernuclei identified in emulsion [11] where binding energy systematic uncertainties are largely canceled out in forming the listed  $\Delta B_{\Lambda}^{\text{exp}}$  values. In the case of the  $({}^7_{\Lambda}\text{He}, {}^7_{\Lambda}\text{Li}^*, {}^7_{\Lambda}\text{Be})$  isotriplet  $\frac{1}{2}^+$  levels shown in Fig. 4, whereas emulsion  $B_{\Lambda}^{\text{exp}}$  (g.s.) values supplemented by the observation of a 3.88 MeV  $\gamma$ -ray transition  ${}^7_{\Lambda}\text{Li}^* \rightarrow \gamma + {}^7_{\Lambda}\text{Li}$  [36] were used for the  ${}^7_{\Lambda}\text{Be}-{}^7_{\Lambda}\text{Li}^*$  pair, recent counter measurements that provide absolute energy calibrations relative to precise values of free-space known masses were used for the  ${}^7_{\Lambda}\text{Li}^*-{}^7_{\Lambda}\text{He}$  pair [27] (FINUDA for  ${}^7_{\Lambda}\text{Li}_{\text{g.s.}}$ ,  $\pi^-$  decay [37] and JLab for  ${}^7_{\Lambda}\text{He}$  electroproduction [38]). Note that the value reported by FINUDA for  $B_{\Lambda}({}^7_{\Lambda}\text{Li}_{\text{g.s.}})$ ,  $5.85 \pm 0.17$  MeV, differs from the emulsion value of  $5.58 \pm 0.05$  MeV. Recent  $B_{\Lambda}$  values from JLab electroproduction experiments for  ${}^9_{\Lambda}\text{Li}$  [39] and  ${}^{10}_{\Lambda}\text{Be}$  [40] were not used for lack of similar data on their mirror partners.

**TABLE 1.**  $\langle V_{\text{CSB}} \rangle$  contributions (in keV) to  $\Delta B_{\Lambda}^{\text{calc}}$  in  $p$ -shell hypernuclei g.s. isomultiplets, using  $\Lambda\Sigma$  coupling matrix elements  $\bar{V}_{\Lambda\Sigma}^{0p}=1.45$  MeV and  $\Delta_{\Lambda\Sigma}^{0p}=3.04$  MeV [21] in Eq. (5). A similar calculation for the  $s$ -shell  $A=4$  mirror hypernuclei [31] is included for comparison. Listed values of  $\Delta B_{\Lambda}^{\text{exp}}$  are based on g.s. emulsion data [11] except for  ${}^4_{\Lambda}\text{He}-{}^4_{\Lambda}\text{H}$  [26] and  ${}^7_{\Lambda}\text{Li}^*-{}^7_{\Lambda}\text{He}$  [27].

${}^A_{\Lambda}Z > - {}^A_{\Lambda}Z <$ $I, J^{\pi}$	${}^4_{\Lambda}\text{He}-{}^4_{\Lambda}\text{H}$ $\frac{1}{2}, 0^+$	${}^7_{\Lambda}\text{Be}-{}^7_{\Lambda}\text{Li}^*$ $1, \frac{1}{2}^+$	${}^7_{\Lambda}\text{Li}^*-{}^7_{\Lambda}\text{He}$ $1, \frac{1}{2}^+$	${}^8_{\Lambda}\text{Be}-{}^8_{\Lambda}\text{Li}$ $\frac{1}{2}, 1^-$	${}^9_{\Lambda}\text{B}-{}^9_{\Lambda}\text{Li}$ $1, \frac{3}{2}^+$	${}^{10}_{\Lambda}\text{B}-{}^{10}_{\Lambda}\text{Be}$ $\frac{1}{2}, 1^-$
$\langle V_{\text{CSB}} \rangle$	232	50	50	119	81	17
$\Delta B_{\Lambda}^{\text{calc}}$	226	-17	-28	+49	-54	-136
$\Delta B_{\Lambda}^{\text{exp}}$	$233 \pm 92$	$-100 \pm 90$	$-20 \pm 230$	$+40 \pm 60$	$-210 \pm 220$	$-220 \pm 250$

The listed  $A = 7 - 10$  values of  $\langle V_{\text{CSB}} \rangle$  exhibit strong SU(4) correlations, highlighted by the enhanced value of 119 keV for the SU(4) nucleon-hole configuration in  ${}^8_{\Lambda}\text{Be}-{}^8_{\Lambda}\text{Li}$  with respect to the modest value of 17 keV for the SU(4) nucleon-particle configuration in  ${}^{10}_{\Lambda}\text{B}-{}^{10}_{\Lambda}\text{Be}$ . This enhancement follows from the relative magnitudes of the Fermi-like interaction term  $\bar{V}_{\Lambda\Sigma}^{0p}$  and its Gamow-Teller partner term  $\Delta_{\Lambda\Sigma}^{0p}$ . Noting that both the  $A = 4$  and  $A = 8$  mirror hypernuclei correspond to SU(4) nucleon-hole configuration, the roughly factor two ratio of  $\langle V_{\text{CSB}} \rangle_{A=4}=232$  keV to  $\langle V_{\text{CSB}} \rangle_{A=8}=119$  keV reflects the approximate factor two ratio of  $0s_N 0s_Y$  to  $0p_N 0s_Y$   $\Lambda\Sigma$  matrix elements. However, in distinction from the  $A=4$  g.s. isodoublet where  $\Delta B_{\Lambda} \approx \langle V_{\text{CSB}} \rangle$ , the increasingly negative Coulomb contributions in the  $p$ -shell overcome the positive  $\langle V_{\text{CSB}} \rangle$  contributions, with  $\Delta B_{\Lambda}$  becoming negative definite for  $A \geq 9$ .

Comparing  $\Delta B_{\Lambda}^{\text{calc}}$  with  $\Delta B_{\Lambda}^{\text{exp}}$  in Table 1, we note the reasonable agreement reached between the  $\Lambda\Sigma$  coupling model calculation and experiment for all five pairs of  $p$ -shell hypernuclei listed here. Extrapolating to heavier hypernuclei, one might naively expect negative values of  $\Delta B_{\Lambda}^{\text{calc}}$ . However, this assumes that the negative Coulomb contribution remains as large upon increasing  $A$  as it is in the beginning of the  $p$  shell, which need not be the case. As nuclear cores beyond  $A = 9$  become more tightly bound, the  $\Lambda$  hyperon is unlikely to compress these nuclear cores as much as it does in lighter hypernuclei, so that the additional Coulomb repulsion in  ${}^{12}_{\Lambda}\text{C}$ , for example, over that in  ${}^{12}_{\Lambda}\text{B}$  may not be sufficiently large to offset the attractive CSB contribution to  $B_{\Lambda}({}^{12}_{\Lambda}\text{C}) - B_{\Lambda}({}^{12}_{\Lambda}\text{B})$ , in agreement with the value  $50 \pm 110$  keV suggested recently for this  $A=12$   $B_{\Lambda}$  (g.s.) splitting using FINUDA and JLab counter measurements [27]. In making this argument one relies on the expectation, based on SU(4) supermultiplet fragmentation patterns in the  $p$  shell, that  $\langle V_{\text{CSB}} \rangle$  does not exceed  $\sim 100$  keV. Based on  $\Lambda\Sigma$  mixing model arguments given in Ref. [41], CSB splittings in medium-heavy and heavy hypernuclei become progressively negligible.

## ${}^3_{\Lambda}\text{H}$ AND ${}^3_{\Lambda}\text{n}$ LIFETIME PUZZLES

Measurements of the  ${}^3_{\Lambda}\text{H}$  lifetime in emulsion or bubble-chamber experiments during the 1960s and early 1970s gave conflicting and puzzling results. Particularly troubling appeared a conference report by Block *et al.* claiming a lifetime of  $\tau({}^3_{\Lambda}\text{H})=(95^{+19}_{-15})$  ps [42], to be compared with a free  $\Lambda$  lifetime  $\tau_{\Lambda}=(236\pm 6)$  ps measured in the same He chamber [43]. Given the loose  $\Lambda$  binding,  $B_{\Lambda}({}^3_{\Lambda}\text{H})=0.13\pm 0.05$  MeV, it was anticipated that  $\tau({}^3_{\Lambda}\text{H})\approx\tau_{\Lambda}$ , as clearly seen in the Rayet and Dalitz (RD) [44] approach in which the  ${}^3_{\Lambda}\text{H}$  decay rate for any of its g.s. doublet members, whichever is the actual g.s., is given by

$$\Gamma_{\Lambda}^{J=1/2} = \frac{\bar{q}}{1 + \omega_{\pi}(\bar{q})/E_{3N}(\bar{q})} [|s_{\pi}|^2 (1 + \frac{1}{2}\eta(\bar{q})) + |p_{\pi}|^2 (\frac{\bar{q}}{q_{\Lambda}})^2 (1 - \frac{5}{6}\eta(\bar{q}))], \quad (6)$$

$$\Gamma_{\Lambda}^{J=3/2} = \frac{\bar{q}}{1 + \omega_{\pi}(\bar{q})/E_{3N}(\bar{q})} [|s_{\pi}|^2 (1 - \eta(\bar{q})) + |p_{\pi}|^2 (\frac{\bar{q}}{q_{\Lambda}})^2 (1 - \frac{1}{3}\eta(\bar{q}))]. \quad (7)$$

Here  $\eta(\bar{q})$ , with values between 0 and 1, is an exchange integral that arises by assigning a fixed pion momentum  $\bar{q}$  in a closure approximation to all pion-nuclear final states. It can be shown that  $\eta(\bar{q}) \rightarrow 0$  when  $B_{\Lambda} \rightarrow 0$ , so apart from minor kinematical factors each  ${}^3_{\Lambda}\text{H}$  decay rate reduces then to the free  $\Lambda \rightarrow N + \pi$  decay rate

$$\Gamma_{\Lambda}(q_{\Lambda}) = \frac{q_{\Lambda}}{1 + \omega_{\pi}(q_{\Lambda})/E_N(q_{\Lambda})} (|s_{\pi}|^2 + |p_{\pi}|^2), \quad \left| \frac{p_{\pi}}{s_{\pi}} \right|^2 \approx 0.132, \quad (8)$$

with  $\omega_{\pi}(q_{\Lambda})$  and  $E_N(q_{\Lambda})$  the center of mass energies of the decay pion and the recoil nucleon, respectively, and where  $q_{\Lambda} \approx 102$  MeV/c is a weighted average for the  $p + \pi^{-}$  and  $n + \pi^0$  branches of the  $\Lambda \rightarrow N + \pi$  weak decay.

**TABLE 2.**  ${}^3_{\Lambda}\text{H}_{\text{g.s.}}(\frac{1}{2}^{+})$  decay rate calculated in units of the free  $\Lambda$  decay rate  $\Gamma_{\Lambda}$  and listed in a year of publication order. The first row lists results for plane-wave pions, disregarding pion final state interaction (FSI) contributions which are listed in the second row. A calculated nonmesonic decay rate contribution of 0.017 from Ref. [45] was added uniformly in obtaining the total decay rates listed in the third row. For a more critical assessment of the decay rates published in Refs. [44, 47], see Ref. [48].

$\Gamma({}^3_{\Lambda}\text{H})$ model	1966 [44]	1992 [46]	1998 [47]	2019 [48]
Without pion FSI	1.05	1.12	1.01	1.11
Pion FSI contribution	-0.013	—	—	0.11
Total	1.05	1.14	1.03	1.23

Table 2 lists  ${}^3_{\Lambda}\text{H}_{\text{g.s.}}(\frac{1}{2}^{+})$  decay rate values calculated by RD and in several subsequent calculations, all reaching similar results. Claims for large departures from the free  $\Lambda$  value are often found incorrect or irreproducible. The RD results were confirmed by Ram and Williams using a wider class of  ${}^3_{\Lambda}\text{H}$  model wavefunctions [49]. The RD methodology was also used in the Congleton [46] and Gal-Garcilazo (GG) [48] calculations, with the latter one solving appropriate three-body Faddeev equations to produce a  ${}^3_{\Lambda}\text{H}$  wavefunction. The Kamada *et al.* calculation [47], while also solving Faddeev equations for the  ${}^3_{\Lambda}\text{H}$  wavefunction, accounted microscopically for the outgoing  $3N$  phase space and FSI, thereby doing without a closure approximation. Pion FSI was considered only in two of these works, with differing results: (i) repulsion, weakly reducing  $\Gamma({}^3_{\Lambda}\text{H})$  in RD; and (ii) attraction, moderately enhancing it in GG. The latter result is supported by the  $\pi^{-}$ -atom  $1s$  level *attractive* shift observed in  ${}^3\text{He}$  [50].

Renewed interest in the  ${}^3_{\Lambda}\text{H}$  lifetime problem arose by recent measurements of  $\tau({}^3_{\Lambda}\text{H})$  in relativistic heavy ion production experiments [51] marked by rectangle systematic uncertainties in Fig. 6. Shown also is the world-average value which is shorter by about 30% than the free- $\Lambda$  lifetime  $\tau_{\Lambda}=(263\pm 2)$  ps. In sharp contrast with the large scatter of old bubble chamber and nuclear emulsion measurements, these five recent measurements of  $\tau({}^3_{\Lambda}\text{H})$  give values persistently shorter by  $(30\pm 8)\%$  than  $\tau_{\Lambda}$ . Also shown in the figure are the  $\tau_{\text{calc}}({}^3_{\Lambda}\text{H})$  values listed in Table 2, all of which are insufficiently short to reproduce the recently measured shorter lifetime values, except the very recent one by ALICE [56]. While enhancement of the free  $\Lambda$  decay rate by up to  $\approx 20\%$  is theoretically conceivable [48], it appears inconceivable to reproduce the 30% or so enhancement suggested by the recent heavy-ion experiments.



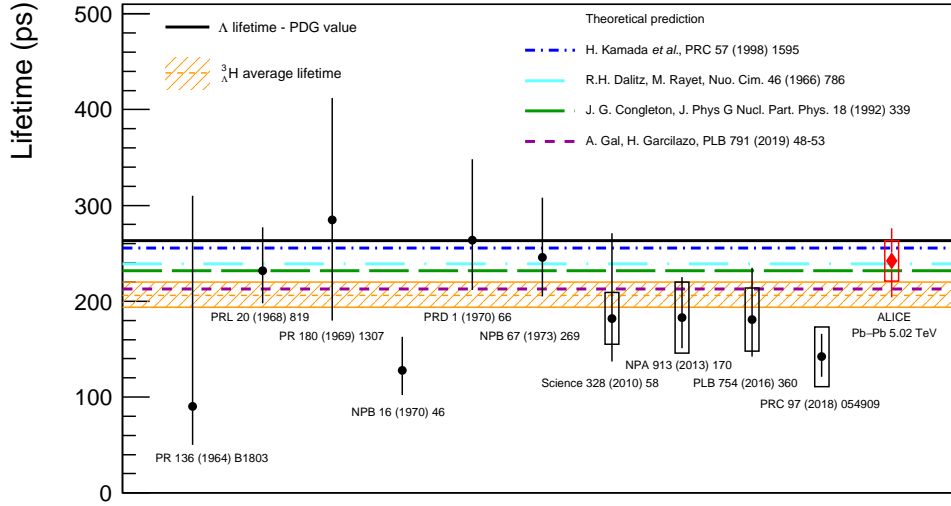


**FIGURE 6.** Compilation of measured  $\Lambda$  lifetime values, plotted in chronological order. The five most recent values are from relativistic heavy ion experiments: STAR [52], HypHI [53], ALICE [54], STAR [55] and ALICE [56]. Shown by horizontal lines are the free- $\Lambda$  lifetime (solid), the world average of measured  $\Lambda$  lifetimes (dashed), and results from the four calculations listed in Table 2. Figure courtesy of Benjamin Dönigus [56].

Before closing this section I wish to make a few remarks on  $\Lambda^3n$ , assuming it is bound as conjectured by the HypHI GSI Collaboration [57] (but unanimously unbound in recent theoretical calculations [58, 59, 60]). In  $\Lambda^3n$  decays induced by  $\Lambda \rightarrow p + \pi^-$ , where the  $\Lambda^3n$  neutrons are spectators, the  $\Lambda^3n \rightarrow (pnn) + \pi^-$  weak decay rate is given in the closure approximation essentially by the  $\Lambda \rightarrow p + \pi^-$  free-space weak-decay rate, whereas in  $\Lambda \rightarrow n + \pi^0$  induced decays the production of a third low-momentum neutron is suppressed by the Pauli principle, and this  $\Lambda^3n$  weak decay branch may be disregarded up to perhaps a few percents. We thus obtain [48]:

$$\Gamma_{\Lambda^3n}^{J=1/2} = \frac{\bar{q}}{1 + \omega_{\pi}(\bar{q})/E_{3N}(\bar{q})} 0.641 \left( |s_{\pi}|^2 + |p_{\pi}|^2 \left( \frac{\bar{q}}{q_{\Lambda}} \right)^2 \right), \quad (9)$$

where the coefficient 0.641 is the free-space  $\Lambda \rightarrow p + \pi^-$  fraction of the total  $\Lambda \rightarrow N + \pi$  weak decay rate. Evaluating the ratio  $\Gamma(\Lambda^3n)/\Gamma_{\Lambda}$  for the choice  $\bar{q} = q_{\Lambda}$  one obtains  $\Gamma(\Lambda^3n)/\Gamma_{\Lambda} \approx 1.114 \times 0.641 = 0.714$ , where the factor 1.114 follows from the difference between  $E_{3N}(q_{\Lambda})$  and  $E_N(q_{\Lambda})$  in the phase space factors, giving rise to an estimated  $\Lambda^3n$  lifetime of  $\tau(\Lambda^3n) \approx 368$  ps, which should hold up to a few percent contribution from the  $\pi^0$  decay branch. This lifetime is considerably longer than  $181_{-24}^{+30} \pm 25$  ps or  $190_{-35}^{+47} \pm 36$  ps deduced from the  $nd\pi^-$  and  $t\pi^-$  alleged decay modes of  $\Lambda^3n$  [57, 61], providing a strong argument against the conjectured stability of  $\Lambda^3n$ .

## $\Lambda^*(1405)$ MATTER?

Recent Lattice QCD calculations [62] demonstrate that the  $\Lambda^*(1405)$   $I = 0$ ,  $J^{\pi} = (1/2)^-$  hyperon is well described by a  $\bar{K}N$  hadronic ‘molecule’, as predicted in 1959 by Dalitz and Tuan [63], rather than by a 3-quark baryon. The observed  $\Lambda^*(1405)$  structure requires a two-pole configuration dominated by a pole closer to the  $\bar{K}N$  threshold than its nominal ‘1405’ position 27 MeV below the  $K^-p$  threshold might suggest [64]. The resulting  $\bar{K}N$  effective potential is then necessarily *energy dependent*, as shown by recent applications of  $\chi$ EFT meson-baryon coupled-channel models that generate it dynamically [65]. The difference between this ‘energy-dependent’  $\bar{K}N$  potential picture and the single-pole ‘energy-independent’  $\bar{K}N$  potential picture advanced by Akaishi and Yamazaki [66, 67] is seen in Table 3 to compound upon going to three- and four-body systems.



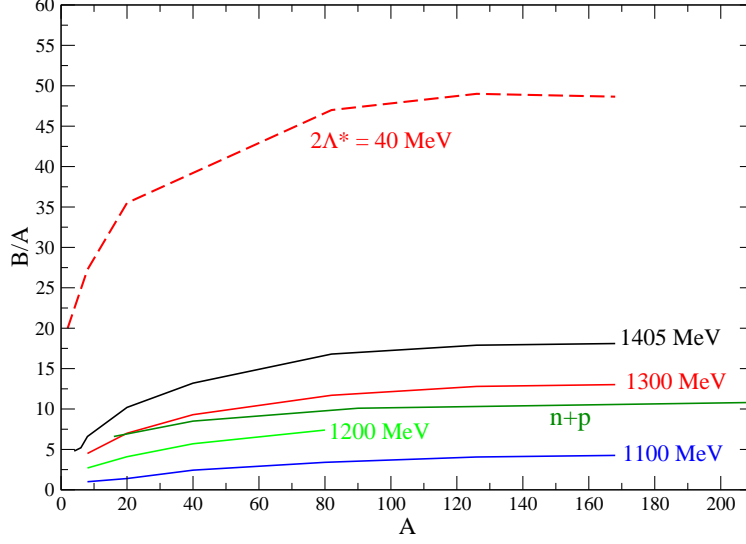


**FIGURE 7.** Binding energies per baryon,  $B/A$ , as a function of mass number  $A$  in RMF calculations [68]. Solid curves use standard nuclear RMF meson-baryon coupling constants [75] for  $n + p$  nuclei and for single-type baryon aggregates with variable mass as marked. The dashed curve for  $\Lambda^*$  aggregates uses an increased scalar coupling constant such that  $B(\Lambda^*\Lambda^*) = 40$  MeV, see Table 3. Figure courtesy of J. Hrtánková and J. Mareš.

The  $\Lambda^*\Lambda^*$  binding energy deduced in Table 3 from the E-indep. calculations [71] is exceptionally large. This was to be expected since the  $\Lambda^*$  itself is a quite strongly bound  $\bar{K}N$  state. It led Akaishi and Yamazaki to speculate, based apparently on non-documented nonrelativistic few-body calculations of  $\Lambda^*$  aggregates, that absolute stability of  $\Lambda^*$  configurations is achieved for  $A \gtrsim 8$  [73]. This speculation dates back to a work coauthored by them in 2004 [74]. What these authors apparently missed was that solving the  $A$ -body Schrödinger equation for purely attractive  $\Lambda^*\Lambda^*$  interactions will necessarily lead to collapse, with the binding energy per  $\Lambda^*$ ,  $B/A$ , and the central  $\Lambda^*$  density  $\rho(r \approx 0)$  diverging as  $A$  increases. The collapse of  $\Lambda^*$  nuclei may be averted within relativistic mean field (RMF) calculations [68], as briefly described below and further detailed by Hrtánková in a separate contribution.

**TABLE 3.**  $(\bar{K}N)_{I=0}$ ,  $(\bar{K}NN)_{I=1/2}$  and  $(\bar{K}\bar{K}NN)_{I=0}$  binding energies  $B$  (in MeV) calculated using energy dependent (E-dep.) and energy independent (E-indep.)  $\bar{K}N$  potentials.  $(\bar{K}\bar{K}NN)_{I=0}$  binding energies are transformed in the last column to  $B_{\Lambda^*\Lambda^*}$  values. Table adapted from [68].

$\bar{K}$ model	$(\bar{K}N)_{I=0}$	$(\bar{K}NN)_{I=1/2}$	$(\bar{K}\bar{K}NN)_{I=0}$	$\Lambda^*\Lambda^*$
(E-dep.) [69]	11.4	15.7	32.1	9.3
(E-dep.) [70]	11	14–28	–	–
(E-indep.) [71]	26.6	51.5	93	40
(E-indep.) [72]	28	51	–	–

Shown in Ref. [68], within RMF calculations in which strongly attractive  $\Lambda^*\Lambda^*$  interactions are generated through scalar meson ( $\sigma$ ) and vector meson ( $\omega$ ) exchanges, is that both  $B/A$  and the central density  $\rho(r \approx 0)$  saturate for values of  $A$  of order  $A \sim 100$ :  $B/A$  saturates at values between roughly 30 to 80 MeV, depending on details of the RMF modeling, and the associated central densities saturate at values about twice nuclear-matter density. A simple example of  $B/A$  saturation is shown in Fig. 7 where the calculated  $\Lambda^*$ -aggregates binding energies (dashed curve) are normalized to yield  $B(\Lambda^*\Lambda^*) = 40$  MeV from Table 3. In these RMF calculations, done for  $\Lambda^*$  closed-shell nuclei, one solves self consistently a coupled system of Klein-Gordon equations for the meson fields and a Dirac equation for  $\Lambda^*$  that result from a  $\Lambda^*$  RMF lagrangian density given by

$$\mathcal{L} = \bar{\Lambda}^* \left[ i\gamma^\mu D_\mu - (M_{\Lambda^*} - g_{\sigma\Lambda^*}\sigma) \right] \Lambda^* + (\sigma, \omega_\mu \text{ free-field terms}), \quad (10)$$

where  $D_\mu = \partial_\mu + i g_{\omega\Lambda^*} \omega_\mu$ ,  $M_{\Lambda^*}$  is the mass of  $\Lambda^*$  and  $g_{i\Lambda^*}$  ( $i = \sigma, \omega$ ) are the corresponding coupling constants.

With calculated values of  $B/A < 100$  MeV,  $\Lambda^*$  aggregates remain highly unstable against strong-interaction decay governed by two-body conversion reactions such as  $\Lambda^* \Lambda^* \rightarrow \Lambda \Lambda, \Sigma \Sigma$ . This preserves the strong-interaction stable form of hadronic matter, known as ‘strange hadronic matter’, in which SU(3)-octet hyperons ( $\Lambda, \Sigma, \Xi$ ) exclusively are as abundant as nucleons [76]. Considering that  $\Lambda^*$ s stand for  $\bar{K}N$  bound states, this conclusion was in fact reached already 10 years ago by Gazda *et al.* in RMF calculations of multi- $\bar{K}$  nuclei, where for a given core nucleus the resulting  $\bar{K}$  separation energies  $B_{\bar{K}}$ , as well as the associated nuclear and  $\bar{K}$ -meson densities, saturate with the number  $\kappa$  of  $\bar{K}$  mesons for  $\kappa \geq 10$  [77]. In these calculations  $B_{\bar{K}}$  generally does not exceed 200 MeV which is insufficient to compete with multi-hyperonic nuclei in providing the ground state of strange hadronic configurations; put differently, it means that kaon condensation is unlikely to occur in strong-interaction self-bound strange hadronic matter.

The RMF calculations discussed above demonstrate the decisive role of Lorentz covariance in producing saturation of binding energies and sizes. Lorentz covariance introduces two types of baryon density, a scalar  $\rho_S = \bar{B}B$  associated with the attractive  $\sigma$  meson field and a vector  $\rho_V = \bar{B}\gamma_0 B$  associated with the repulsive  $\omega$  meson field. Whereas  $\rho_V$  coincides with the conserved baryon density  $B^\dagger B$ ,  $\rho_S$  shrinks with respect to  $\rho_V$  in dense matter by a multiplicative factor  $M^*/E^* < 1$ , where  $M^* = M - g_{\sigma B} \langle \sigma \rangle < M$  is the baryon density-dependent effective mass, thereby damping the attraction from the scalar  $\sigma$  meson field and maintaining saturation. In contrast, non-relativistic calculations with static potentials that underlie the standard RMF nuclear calculations would lead to collapse of systems composed of sufficiently large number of  $\Lambda^*$  baryons, as it also holds for nucleons (M. Schäfer, private communication).

## SUMMARY

Here I comment briefly on three of the four topics discussed in earlier sections.

**Overbinding in  $\Lambda$  hypernuclei.** The discussion above made it clear that  $\Lambda NN$  repulsive interactions are required to resolve the overbinding problem of  ${}^5_\Lambda\text{He}$ . One may ask whether these  $\Lambda NN$  interaction terms are of similar magnitude to those used by the QMC practitioners across the periodic table, namely  $\Lambda NN$  (I,II) in Fig. 2. The figure suggests that their two-body attractive  $\Lambda N$  interaction is exceedingly strong, perhaps leading on its own to a  $\Lambda$  well depth of order  $D_\Lambda^{(2)} \gtrsim 100$  MeV. If so, the compensating  $\Lambda NN$  repulsive interaction is also huge, canceling most of the  $\Lambda N$  attraction in reaching the phenomenologically deduced value of  $D_\Lambda \sim 30$  MeV. To estimate  $D_\Lambda^{(2)}$ , one starts from the 1st order  $\Lambda$ -nucleus optical potential ‘ $t\rho$ ’ form, including long-range Pauli correlations [78],

$$V_\Lambda(\rho) = -\frac{4\pi}{2m_\Lambda} a_{\Lambda N}^{\text{lab}}(\rho) \rho, \quad a_{\Lambda N}^{\text{lab}}(\rho) = \frac{a_{\Lambda N}^{\text{lab}}}{1 + (3/2\pi)k_F(\rho)a_{\Lambda N}^{\text{lab}}}, \quad (11)$$

in terms of a nuclear-medium Pauli corrected  $\Lambda N$  scattering length  $a_{\Lambda N}^{\text{lab}}(\rho)$  and nuclear density  $\rho = 2k_F^3/3\pi^2$  where  $k_F$  is the local Fermi momentum. It was assumed that the singlet and triplet  $\Lambda N$  scattering lengths assume the same value which is taken directly from the Alexander *et al.*  $\Lambda p$  scattering experiment [16]:  $a_{\Lambda N}^{\text{cm}} = 1.65$  fm. For nuclear-matter density  $\rho_0 = 0.170$  fm $^{-3}$  corresponding to Fermi momentum  $k_F = 1.36$  fm $^{-1}$ , one obtains  $D_\Lambda^{(2)} = -V_\Lambda(\rho) = 40.2$  MeV which roughly in the range of values reached using Nijmegen soft-core and extended soft core potentials [79], but much smaller than the value reached by the QMC practitioners. This observation requires further studies.

**CSB in hypernuclei.** It was shown above that the Gazda-Gal calculations [29, 30] of the  ${}^4_\Lambda\text{He}$ - ${}^4_\Lambda\text{H}$  binding energy difference in the  $0^+$  g.s. were able to reproduce the order of magnitude around 200 keV of this CSB splitting using a simple prescription, Eq. (2), suggested by  $\Lambda - \Sigma^0$  mixing. This mixing induces a long-range OPE CSB interaction related via (2) to the strong-interaction OPE  $\Lambda\Sigma$  coupling. Other hadron mixings,  $\omega - \rho^0$  and  $\eta - \pi^0$ , generate considerably shorter-range CSB potentials that apparently are much weaker than the OPE potential induced by  $\Lambda - \Sigma^0$  mixing. In the  $A=3$  core nuclei, the  ${}^3\text{H}$ - ${}^3\text{He}$  binding energy difference of 764 keV is dominated by the Coulomb interaction, leaving about 70 keV to CSB which is believed to arise mostly from  $\omega - \rho^0$  mixing [80]. Considering that only  $\omega$ , but not  $\rho^0$  couples to  $\Lambda$ , and that the  $\omega\Lambda$  coupling constant is roughly 2/3, in SU(6), of the  $\omega N$  coupling constant, the  $\omega - \rho^0$  mixing effect in the  $A=4$  hypernuclei should be roughly 1/3 of its contribution in the  $A=3$  nuclei, namely about 20 keV in size. Indeed, this is close to the  $\omega - \rho^0$  mixing contribution in the  $A=4$  hypernuclei reported by Coon *et al.* [81] who also found even a smaller  $\eta - \pi^0$  contribution. In conclusion, it appears that the CSB interaction operative in  $\Lambda$  hypernuclei is dominated by the OPE component generated by  $\Lambda - \Sigma^0$  mixing.

**Lifetimes of light hypernuclei.** It was shown that a lifetime of  ${}^3_{\Lambda}\text{H}$  shorter by up to  $\approx 20\%$  than the free  $\Lambda$  lifetime may be accommodated by theory. A new theoretical development is the  $\sim 10\%$  estimated contribution from the attractive pion FSI for  $A=3$  [48]. If confirmed, and perhaps found even somewhat larger, it might bridge the gap between our present  $\approx 20\%$  theoretical estimate for the reduction of  $\tau({}^3_{\Lambda}\text{H})$  with respect to  $\tau_{\Lambda}$  and the  $\approx 30\%$  reported in relativistic heavy-ion collision experiments. It is remarkable that  ${}^3_{\Lambda}\text{H}$  decay is the only light hypernucleus decay where the pion FSI is expected to be attractive. The decays of  ${}^4_{\Lambda}\text{H}$ ,  ${}^4_{\Lambda}\text{He}$  and  ${}^5_{\Lambda}\text{He}$  involve pion- ${}^4\text{He}$  FSI which is known from the  $\pi^-$  atomic  ${}^4\text{He}$   $1s$  level shift to be repulsive [82]. Disregarding such pion FSI in the decay of the  $A=4$  hypernuclei, simple estimates of their lifetimes agree well with the KEK measured values [83]:

$$\tau({}^4_{\Lambda}\text{H}) = 194^{+24}_{-26} \text{ ps}, \quad \tau({}^4_{\Lambda}\text{He}) = 256 \pm 27 \text{ ps}. \quad (12)$$

The difference between these lifetimes arises mostly from the difference between the strongest partial decays which are the two-body decays to  $\pi+{}^4\text{He}$ , with a rate calculated reliably as  $\approx 0.7\Gamma_{\Lambda}$  for  ${}^4_{\Lambda}\text{H}$  and half of that for  ${}^4_{\Lambda}\text{He}$ , reflecting the  $\pi^-$  to  $\pi^0$  weights in the free  $\Lambda$  decay. Hence the difference between the  ${}^4_{\Lambda}\text{H}$  and  ${}^4_{\Lambda}\text{He}$  total decay rates should amount to  $\approx 0.35\Gamma_{\Lambda}$ , close to the  $\approx 0.33\Gamma_{\Lambda}$  given by the measured lifetimes (12).

## ACKNOWLEDGMENTS

Many thanks are due to Liguang Tang and his JLab organizing team for the gracious hospitality bestowed on me during the HYP2018 International Conference at Portsmouth-Norfolk, VA. I am also indebted to my good colleagues Nir Barnea, Lorenzo Contessi, Eli Friedman, Humberto Garcilazo, Daniel Gazda, Jaroslava Hrtánková, Jiří Mareš, John Millener, Moreh Nevuchim, and Martin Schäfer for many insights gained through our long-standing collaborations.

## REFERENCES

- [1] A. Gal, E.V. Hungerford, and D.J. Millener, *Rev. Mod. Phys.* **88**, 035004 (2016).
- [2] H. Hotchi, *et al.*, *Phys. Rev. C* **64**, 044302 (2001).
- [3] D.J. Millener, C.B. Dover, and A. Gal, *Phys. Rev. C* **38**, 2700 (1988).
- [4] P. Pile, *et al.*, *Phys. Rev. Lett.* **66**, 2585 (1991).
- [5] J.P. Lagnaux, *et al.*, *Nucl. Phys.* **60**, 97 (1964).
- [6] J. Lemonne, *et al.*, *Phys. Lett.* **18**, 354 (1965).
- [7] D. Lonardoni, F. Pederiva, and S. Gandolfi, *Phys. Rev. C* **89**, 014314 (2014).
- [8] D. Lonardoni, A. Lovato, S. Gandolfi, and F. Pederiva, *Phys. Rev. Lett.* **114**, 092301 (2015).
- [9] W. Weise, *Hyperfine Interactions* **233**, 131 (2015); T. Hell and W. Weise, *Phys. Rev. C* **90**, 045801 (2014).
- [10] R.H. Dalitz, R.C. Herndon, and Y.C. Tang, *Nucl. Phys. B* **47**, 109 (1972).
- [11] D.H. Davis, *Nucl. Phys. A* **754**, 3 (2005).
- [12] M. Raymund, *Nuovo Cimento* **32**, 555 (1964).
- [13] D. Lonardoni, S. Gandolfi, and F. Pederiva, *Phys. Rev. C* **87**, 041303(R) (2013).
- [14] R. Wirth, and R. Roth, *Phys. Lett. B* **779**, 336 (2018).
- [15] L. Contessi, N. Barnea, and A. Gal, *Phys. Rev. Lett.* **121**, 102502 (2018); and in this Volume.
- [16] G. Alexander, *et al.*, *Phys. Rev.* **173**, 1452 (1968).
- [17] H. Polinder, J. Haidenbauer, and U.-G. Meißner, *Nucl. Phys. A* **779**, 244 (2006).
- [18] A. Nogga, H. Kamada, and W. Glöckle, *Phys. Rev. Lett.* **85**, 944 (2000).
- [19] A. Gal, J.M. Soper, and R.H. Dalitz, *Ann. Phys. (N.Y.)* **63**, 53 (1971); in particular Eq. (5.2) therein.
- [20] D.J. Millener, A. Gal, C.B. Dover, and R.H. Dalitz, *Phys. Rev. C* **31**, 499 (1985).
- [21] D.J. Millener, *Nucl. Phys. A* **881**, 298 (2012).
- [22] R. Wirth and R. Roth, *Phys. Rev. Lett.* **117**, 182501 (2016).
- [23] A. Gal, *Phys. Rev. Lett.* **18**, 568 (1967).
- [24] T.O. Yamamoto, *et al.* (J-PARC E13 Collaboration), *Phys. Rev. Lett.* **115**, 222501 (2015).
- [25] A. Esser, *et al.* (MAMI A1 Collaboration), *Phys. Rev. Lett.* **114**, 232501 (2015).
- [26] F. Schulz, *et al.* (MAMI A1 Collaboration), *Nucl. Phys. A* **954**, 149 (2016).
- [27] E. Botta, T. Bressani, and A. Feliciello, *Nucl. Phys. A* **960**, 165 (2017).
- [28] R.H. Dalitz and F. Von Hippel, *Phys. Lett.* **10**, 153 (1964).

- [29] D. Gazda and A. Gal, Phys. Rev. Lett. **116**, 122501 (2016).
- [30] D. Gazda and A. Gal, Nucl. Phys. A **954**, 161 (2016).
- [31] A. Gal, Phys. Lett. B **744**, 352 (2015).
- [32] D. Gazda, J. Mareš, P. Navrátil, R. Roth, and R. Wirth, Few-Body Syst. **55**, 857 (2014).
- [33] Th.A. Rijken, V.G.J. Stoks, and Y. Yamamoto, Phys. Rev. C **59**, 21 (1999).
- [34] A. Akaishi, T. Harada, S. Shinmura, and K.S. Myint, Phys. Rev. Lett. **84**, 3539 (2000).
- [35] A. Gal and D. Gazda, J. Phys. Conf. Series **966**, 012006 (2018).
- [36] H. Tamura, *et al.*, Phys. Rev. Lett. **84**, 5963 (2000).
- [37] M. Agnello, *et al.* (FINUDA Collaboration and A. Gal), Phys. Lett. B **681**, 139 (2009).
- [38] T. Gogami, *et al.* (JLab HKS Collaboration), Phys. Rev. C **94**, 021302(R) (2016).
- [39] G.M. Urciuoli, *et al.* (JLab Hall A Collaboration), Phys. Rev. C **91**, 034308 (2015).
- [40] T. Gogami, *et al.* (JLab HKS Collaboration), Phys. Rev. C **93**, 034314 (2016).
- [41] A. Gal and D.J. Millener, Phys. Lett. B **725**, 445 (2013).
- [42] M.M. Block, *et al.*, Proc. Sienna Int'l. Conf. on Elementary Particles, Vol. **1**, 63 (Bologna 1963).
- [43] M.M. Block, *et al.*, Phys. Rev. **130**, 766 (1963).
- [44] M. Rayet and R.H. Dalitz, Nuovo Cimento **46A**, 786 (1966).
- [45] J. Golak, K. Miyagawa, H. Kamada, H. Witała, W. Glöckle, A. Parreño, A. Ramos, and C. Bennhold, Phys. Rev. C **55**, 2196 (1997); Erratum: Phys. Rev. C **56**, 2892 (1997).
- [46] J.G. Congleton, J. Phys. G **18**, 339 (1992).
- [47] H. Kamada, J. Golak, K. Miyagawa, H. Witała, and W. Glöckle, Phys. Rev. C **57**, 1595 (1998).
- [48] A. Gal and H. Garcilazo, Phys. Lett. B **791**, 48 (2019).
- [49] B. Ram and W. Williams, Nucl. Phys. B **28**, 566 (1971).
- [50] I. Schwanner, *et al.*, Nucl. Phys. A **412**, 253 (1984).
- [51] P. Braun-Munzinger and B. Dönigus, Nucl. Phys. A **987**, 144 (2019).
- [52] B.I. Abelev, *et al.* (STAR Collaboration), Science **328**, 58 (2010).
- [53] C. Rappold, *et al.* (HypHI Collaboration), Nucl. Phys. A **913**, 170 (2013).
- [54] J. Adam, *et al.* (ALICE Collaboration), Phys. Lett. B **754**, 360 (2016).
- [55] L. Adamczyk, *et al.* (STAR Collaboration), Phys. Rev. C **97**, 054909 (2018).
- [56] S. Acharya, *et al.* (ALICE Collaboration), submitted to Phys. Lett. B, arXiv:1907.06906, preliminarily in S. Trogolo (on behalf of the ALICE Collaboration), Nucl. Phys. A **982**, 815 (2019).
- [57] C. Rappold, *et al.* (HypHI Collaboration), Phys. Rev. C **88**, 041001(R) (2013).
- [58] H. Garcilazo and A. Valcarce, Phys. Rev. C **89**, 057001 (2014).
- [59] E. Hiyama, S. Ohnishi, B.F. Gibson, and Th.A. Rijken, Phys. Rev. C **89**, 061302(R) (2014).
- [60] A. Gal and H. Garcilazo, Phys. Lett. B **736**, 93 (2014).
- [61] T. Saito, *et al.* (HypHI Collaboration), Nucl. Phys. A **954**, 199 (2016).
- [62] J.M.M. Hall, *et al.*, Phys. Rev. Lett. **114**, 132002 (2015).
- [63] R.H. Dalitz and F.S. Tuan, Phys. Rev. Lett. **2**, 425 (1959).
- [64] U.-G. Meißner and T. Hyodo, *Pole Structure of the  $\Lambda(1405)$  Region*, a PDG18 Review in M. Tanabashi, *et al.*, Phys. Rev. D **98**, 030001 (2018).
- [65] K. Miyahara, T. Hyodo, and W. Weise, Phys. Rev. C **98**, 025201 (2018), and references listed therein.
- [66] Y. Akaishi and T. Yamazaki, Phys. Rev. C **65**, 044005 (2002).
- [67] T. Yamazaki and Y. Akaishi, Phys. Rev. C **76**, 045201 (2007).
- [68] J. Hrtánková, N. Barnea, E. Friedman, A. Gal, J. Mareš, and M. Schäfer, Phys. Lett. B **785**, 90 (2018); and in this Volume.
- [69] N. Barnea, A. Gal, and E.Z. Liverts, Phys. Lett. B **712**, 132 (2012).
- [70] A. Doté, T. Inoue, T. Myo, Phys. Lett. B **784**, 405 (2018).
- [71] S. Maeda, Y. Akaishi, and T. Yamazaki, Proc. Jpn. Acad. Ser. B **89**, 418 (2013).
- [72] A. Doté, T. Inoue, T. Myo, Phys. Rev. C **95**, 062201(R) (2017).
- [73] Y. Akaishi and T. Yamazaki, Phys. Lett. B **774**, 522 (2017).
- [74] T. Yamazaki, Y. Akaishi, and A. Doté, Phys. Lett. B **587**, 167 (2004).
- [75] C.J. Horowitz and B.D. Serot, Nucl. Phys. A **368**, 503 (1981).
- [76] J. Schaffner, C.B. Dover, A. Gal, C. Greiner, and H. Stöcker, Phys. Rev. Lett. **71**, 1328 (1993); J. Schaffner, C.B. Dover, A. Gal, C. Greiner, D.J. Millener, and H. Stöcker, Ann. Phys. **235**, 35 (1994); J. Schaffner-Bielich and A. Gal, Phys. Rev. C **62**, 034311 (2000).
- [77] D. Gazda, E. Friedman, A. Gal, and J. Mareš, Phys. Rev. C **77**, 045206 (2008).
- [78] T. Waas, M. Rho, and W. Weise, Nucl. Phys. A **617**, 449 (1997).
- [79] H.-J. Schulze and T. Rijken, Phys. Rev. C **88**, 024322 (2013).
- [80] G.A. Miller, A.K. Opper, and E.J. Stephenson, Annu. Rev. Nucl. Part. Sci. **56**, 253 (2006).
- [81] S.A. Coon, H.K. Han, J. Carlson, and B.F. Gibson, in *Proceedings of Meson and Light Nuclei '98* edited by J. Adam, *et al.* (WS, Singapore, 1999), pp. 407-413.
- [82] G. Backenstoss, *et al.*, Nucl. Phys. A **232**, 519 (1974).
- [83] H. Outa, *et al.*, Nucl. Phys. A **639**, 251 (1998).